Aerosol Assisted Chemical Vapor Deposition of Gold and Nanocomposite Thin Films from Hydrogen Tetrachloroaurate(III)

Robert G. Palgrave and Ivan P. Parkin*

Materials Chemistry Research Centre, Department of Chemistry, University College London, 20 Gordon Street, London WC1H 0AJ, U.K.

Received December 7, 2006. Revised Manuscript Received May 15, 2007

Hydrogen tetrachloroaurate ($HAuCl_4$) has been investigated as a precursor to gold films using aerosol assisted CVD. [$HAuCl_4$] proved to be an excellent precursor to metallic gold, yielding films under a wide range of conditions with tunable optical properties. In addition, gold particles have been incorporated into several different transition metal oxide thin films (TiO_2, WO_3, and MoO_3) using a single step process. The films were deposited onto silica glass using [$Ti(O^iPr)_4$], [$W(CO)_6$], [$Mo(CO)_6$], and [$HAuCl_4$] as precursors, and acetone, methanol, and toluene as solvents. Substrate temperatures from 200 to 400 °C were used. XRD and XPS confirmed the presence of metallic gold and metal oxide within the films. The concentration of gold within the films could be varied widely; the Au:M (M = Ti, W, Mo) atomic ratio ranged from 0.1 to 1.9 depending on the initial precursor ratio. Films showed optical properties characteristic of gold nanocomposite materials: surface plasmon resonance (SPR) absorption peaks and metal-like reflectivity. The frequency and intensity of the SPR absorption was found to be dependent on the concentration of gold particles within the film and the refractive index of the metal oxide matrix.

Introduction

Materials comprising group 11 metal nanoparticles contained within an inert matrix have been of great research interest. Nanoscale Cu, Ag, and Au particles display surface plasmon resonance in the visible region, which has led to their use in optical devices.[1−4] Insulating matrix materials such as organic polymers have been extensively investigated,[2−4] as have semiconducting transition metal oxides. Transition metal oxides are known to display a wide variety of functional properties, including catalysis, electrochromism, and thermochromism.[5−7] Biphasic nanocomposites can display properties characteristic of both phases. Importantly, their physical and chemical properties can be altered by changing the size, shape, and distribution of the nanoscale phase. Therefore, these materials can be tuned to a desired set of material properties through relatively minor changes in their nanostructure.[8] Several potential applications for nanocomposite have been identified and investigated, including photovoltaic cells, gas sensors, and catalysts.[1] Recent interest in group 11 metal/metal oxide nanocomposite materials has been driven by advances in understanding of their optical and functional properties,[8,9] and by the development of new synthetic methods.[10]

We have previously reported the deposition of gold nanocomposite films from a preformed gold nanoparticle solution and a suitable conventional precursor using an aerosol assisted CVD (AACVD) technique.[11] In addition, conventional thermal CVD has also been used to deposit gold films; however, volatile gold precursors are required. Established volatile gold precursors, for example organo-gold phosphine and cyano complexes[12−14] and gold carboxylate complexes,[15] are effective but can be difficult to synthesize and handle as they are usually air and moisture sensitive. Incorporation of impurities may also be a problem with organo-gold precursors, although this has been overcome by the use of fluorinated ligands.[15,16] Inorganic gold precursors are generally more stable and give cleaner decomposition, but they tend to be less volatile, requiring elevated temperatures and reduced pressure.[16] Composite films containing Au have been produced by a variety of methods, including spin coating and dip coating,[17−20] sol−gel deposition,[21,22]

* To whom correspondence should be addressed. E-mail: i.p.parkin@ucl.ac.uk.

(1) Armelao, L; Barreca, D.; Bottaro, G.; Gasparotto, A.; Gross, S.; Maragno, C.; Tondello, E. *Coord. Chem. Rev.* **2006**, *250*, 1294.
(2) Kiesow, A.; Morris, J. E.; Radehaus, C.; Heilmann, A. *J. Appl. Phys.* **2003**, *94*, 6988.
(3) Heilmann, A.; Quinten, M.; Werner, J. *Eur. Phys. J. B* **1998**, *3*, 455.
(4) Heilmann, A. *Polymer Films with Embedded Metal Nanoparticles*; Springer: Berlin, 2003.
(5) O'Neill, S.; Parkin, I. P.; Clark, R. J. H.; Mills, A.; Elliot, N. *Chem. Vap. Deposition* **2004**, *10*, 136.
(6) Mills, A.; Hill, G.; Bhopal, S.; Parkin, I. P.; O'Neill, S. A. *J. Photochem. Photobiol., A* **2003**, *160*, 185.
(7) Ashraf, S.; Blackman, C. S.; Hyett, G.; Parkin, I. P. *J. Mater. Chem.* **2006**, *16*, 3575.
(8) Ung, T.; Liz-Marzan, L. M.; Mulvaney, P. *J. Phys. Chem B* **2001**, *105*, 3441.
(9) Ung, T.; Liz-Marzan, L. M.; Mulvaney, P. *Colloids Surf., A* **2002**, *202*, 119.
(10) Armelao, L; Barreca, D.; Bottaro, G.; Gasparotto, A.; Tondello, E.; Ferroni, M.; Polizzi, S. *Chem. Mater.* **2004**, *16*, 3331.
(11) Palgrave, R. G.; Parkin, I. P. *J. Am. Chem. Soc.* **2006**, *128*, 1587.
(12) Dryden, N. H.; Shapter, J. G.; Coatsworth, L. L.; Norton, P. R.; Puddephatt, R. J. *Chem. Mater.* **1992**, *4*, 979.
(13) Puddephatt, R. J.; Treurnicht, I. *J. Organomet. Chem.* **1987**, *319*, 129.
(14) Szøyk, E.; Piszczek, P.; Lakomska, I.; Grodzicki, A.; Szatkowski, J.; Bøaszczyk, T. *Chem. Vap. Deposition* **2000**, *6*, 3.
(15) Grodzicki, A.; Lakomska, I.; Piszczek, P.; Szymanska, I.; Szlyk, E. *Coord. Chem. Rev.* **2005**, *249*, 2232.
(16) Hampden-Smith, M. J.; Kodas, T. T. *Chem. Vap. Deposition* **1995**, *1*, 8.
(17) Subramanian, V.; Wolf, E. E.; Kamat, P. V. *J. Am. Chem. Soc.* **2004**, *126*, 4943.

10.1021/cm0629006 CCC: $37.00
Published on Web 08/18/2007

ultrasonic insertion,[23] and layer by layer deposition of core−shell nanoparticles.[8,9] CVD fabrication has a number of advantages, including deposition of robust, adherent, conformal films, with the possibility of industrial scale production.

Here we describe a fundamentally new approach with a new precursor set for the formation of nanoparticle and nanoparticle/semiconductor composite films by chemical vapor deposition (CVD). The method is based on aerosol assisted CVD which uses a liquid−gas aerosol to transport soluble precursors to a heated substrate at atmospheric pressure. AACVD requires soluble precursors rather than volatile ones, so the range of viable precursors is significantly shifted compared with standard atmospheric pressure CVD techniques. As a consequence, we were able to investigate hydrogen tetrachloroaurate ($HAuCl_4$) as a CVD precursor to metallic gold. [$HAuCl_4$] is unsuitable for atmospheric pressure CVD (APCVD) as it has poor volatility and decomposes at around 175 °C. It has, however, been used extensively in the solution-phase synthesis of gold nanoparticles, as it is easily reduced to metallic gold.[24,25] The thermal decomposition of [$HAuCl_4$] is expected to proceed as follows:

$$HAuCl_4 \rightarrow Au(s) + HCl(g) + {}^3/_2Cl_2(g)$$

The production of a single solid phase with gaseous byproducts is a desirable decomposition pathway for a CVD precursor. We show here that hydrogen tetrachloroaurate is an excellent precursor to metallic gold, depositing gold nanoparticle films when used alone, and composite films when deposited in conjunction with a second precursor. We have investigated depositing gold in conjunction with [$W(CO)_6$], [$Mo(CO)_6$], and [$Ti(O^iPr)_4$] forming nanocomposite films of Au:WO_3, Au:MoO_3, and Au:TiO_2, respectively. This range of metal oxides was chosen as each has functional properties, such as thermochromism, photochromism, and catalysis, which have been investigated in thin film form.[5−7] The concentration of gold and hence the absorption and reflection properties of the films could be varied by using different precursor concentrations. Our deposition strategy uses precursors that are relatively inexpensive, readily available from chemical suppliers, and, most importantly, easy to handle. Furthermore, in comparison to our earlier paper, there was no need to synthesize nanoparticles in a separate step prior to the CVD process.[11] A range of gold/semiconductor nanocomposite films can now be inexpensively produced by the method presented here.

Experimental Section

All chemicals were obtained from Aldrich Chemical Co. and were of the highest purity available. Two types of deposition were carried out: gold nanoparticle films were deposited from $HAuCl_4$ dissolved in methanol, and composite films were deposited from a solution of [$HAuCl_4$] and a second precursor. These precursor solutions were prepared by dissolving the required precursors ([$W(CO)_6$], [$Mo(CO)_6$], [$Ti(O^iPr)_4$], [$HAuCl_4$]) in either methanol, acetone, or toluene. This range of solvents was necessary due to the different solubility of the precursors. In the case of toluene depositions, $HAuCl_4$ was first dissolved in deionized water, and then stirred vigorously with a 50 mM solution of tetraoctylammonium bromide (TOAB) in toluene. Upon stirring, the toluene layer immediately became dark orange in color, indicating the phase transfer of the Au^{3+} ions to the organic phase.

Depositions were carried out in a cold-wall horizontal-bed CVD reactor. A substrate and top plate were used. These were of dimensions 145 × 45 × 5 mm^3 and were supplied by Pilkington Plc. Films were deposited on one side of the glass only. Gold nanoparticle films were deposited on silica glass coated with a conducting SnO_2 layer; the transparent conducting substrate was chosen to aid microscopic and spectroscopic analysis. Composite films were deposited onto a SiO_2 barrier layer in order to prevent migration of metal ions into the film. In both cases, the substrate rested on a carbon heating block powered by a Whatmann cartridge heater, the temperature monitored by Pt−Rh thermocouples. A top plate was positioned parallel to the substrate and 8 mm above it, and the whole assembly was contained within a quartz tube. An aerosol was generated from the precursor solution in a glass flask using a Vicks ultrasonic humidifier. The aerosol was directed to the reactor by nitrogen gas (BOC) through poly(tetrafluoroethylene) (PTFE) tubing, entering the reactor between the top plate and substrate; reactor waste left via an exhaust port. The gas flow was continued until all the precursor mix had passed through the reactor, typically taking 20−30 min depending on the gas flow rate. Films were cooled in situ under a flow of nitrogen gas, and subsequently were handled and stored in air. Thermogravimetric analysis (TGA) was carried out on [$HAuCl_4$] using a NETZCH STA-449C instrument; a heating rate of 10 K min^{-1} in a nitrogen atmosphere was used.

Film Analysis. X-ray photoelectron spectroscopy (XPS) measurements were carried out on a VG ESCALAB 220i XL instrument using monochromatic Al Kα radiation. Binding energies were referenced to surface elemental carbon 1s peak with binding energy 284.6 eV in order to compensate for the effects of charging. UV−vis spectra were obtained using a Thermo Helios-α spectrometer. Reflectance measurements were taken on a Perkin-Elmer Lambda 950 UV−vis spectrometer. Reflectance measurements were taken at normal incidence and were standardized relative to Spectralon standards. Scanning electron microscopy (SEM) was carried out using a JEOL 6301F instrument using voltages between 6 and 15 kV, at 8 μA. Powder X-ray Diffraction was undertaken using a Bruker-Axs D8 (GADDS) diffractometer. This instrument uses a 2D area X-ray detector to record large sections of multiple Debye−Scherrer cones simultaneously. After collection, the data can be integrated to produce a standard one-dimensional diffractogram. The instrument uses a Cu Kα X-ray source which is collimated such that only a small area of the sample (approximately 3−4 mm^2) is illuminated by the beam at any one time. This allows several small spots on the film to be analyzed separately. To record diffraction peaks from the thin films, a fixed incidence angle of 5° was used. The amount of gold deposition was approximated at various points on a given substrate through determination of the area of the Au(111) diffraction peak. This technique is based on the assumption that the gold is present in crystallite sizes detectable by powder-XRD, and several further assumptions, discussed below. For these experiments, identical experimental parameters were used

(18) He, T.; Ma, Y.; Cao, Y.; Yang, W.; Yao., J. *Phys. Chem. Chem. Phys.* **2002**, *4*, 1637.
(19) He, T.; Ma, Y.; Cao, Y.; Yang, W.; Yao, J. *J. Electroanal. Chem.* **2001**, *514*, 129.
(20) Tian, Y.; Tatsuma, T. *Chem. Commun.* **2004**, 1810.
(21) Hida, Y.; Kozuka, H. *Thin Solid Films* **2005**, *476*, 264.
(22) Yang, Y.; Shi, J.; Huang, W.; Dai, S.; Wang, L. *J. Mater. Sci.* **2003**, *38*, 1243.
(23) Wang, X.; Yu, J. C.; Ho, C.; Mak, A. C. *Chem. Commun.* **2005**, 2262.
(24) Brust, M.; Walker, M.; Bethell, D.; Schiffrin, D. J.; Whyman, R. *J. Chem. Soc., Chem. Commun.* **1994**, 801.
(25) Chen, S. H.; Kimura, K., *Langmuir* **1999**, *15*, 1075.

for the collection of each diffraction pattern: an X-ray incident angle ($\theta 1$) of 5° and a detector angle ($\theta 2$) of 30° were used. Data was collected for a period of 600 s in each case. The sample was moved using the motorized stage, allowing accurate positioning. At each point the height sample was manually adjusted to ensure correct focusing of the X-ray beam. These manual adjustments were small, approximately 0.1 mm. The Au(111) peak was integrated using a linear baseline to quantify the amount of crystalline gold present at each point. Since the area of the sample that is irradiated is the same in each case, the integrated peak area is related to the film thickness, assuming the film has good crystallinity, and no variation in texture and uniform porosity. It has been reported that gold crystallites as small as 3.0 nm give well resolved powder XRD peaks, indicating that this method should be applicable to even nanocrystalline gold films.[25] Reflectance spectra were obtained on a Perkin-Elmer Lambda 950 instrument using normal incidence.

Results

Gold Micro- and Nanoparticle Films. Thermogravimetric analysis was carried out to investigate the decomposition of the precursor. TGA of $HAuCl_4$ showed mass losses associated with decomposition to metallic gold. Two separate steps could be identified; the first between 80 and 110 °C represented a mass loss of 8.2%, close to the expected mass change for the loss of HCl (10.7%). The second step occurred between 150 and 200 °C, and represented a mass loss of 30.9%, very close to the expected change on loss of $^3/_2Cl_2$ (31.3%). The mass was constant after 300 °C, and the total mass loss correlates well with the decomposition of the precursor to metallic gold.

Gold films were deposited using a solution of hydrogen tetrachloroaurate in methanol. In general, depositions using hydrogen tetrachloroaurate gave reproducible films at a wide range of temperatures and concentrations, and in a variety of solvents. [$HAuCl_4$] appears to be an excellent CVD precursor, which has, until now, been overlooked due to its poor volatility. Initial investigations identified that good coverage of the substrate could be achieved using a precursor solution made up of $HAuCl_4 \cdot 3H_2O$ (0.080 g, 0.2 mmol) in methanol (50 mL) using a substrate temperature of 500 °C and a flow rate of 2.0 L min^{-1}. This set of conditions was used as a basis for investigating the effects of varying the substrate temperature and precursor concentration.

The substrate temperature was varied between 400 and 600 °C. At 400 °C, the gold films appeared light blue in transmitted light with a metallic gold luster in reflected light. The films were not physically robust, and could be removed from the glass with slight mechanical abrasion. At 500 °C, gold films appeared dark blue in transmitted light, with a gold luster in reflection. The films were adherent and undamaged by routine handling or wiping with a tissue. At 600 °C the films were blue/purple in transmitted light, with some areas of powdery yellow deposition. The powdery deposition was nonadherent and could easily be rubbed off the glass, while the purple areas were more resistant to abrasion. At the higher deposition temperatures, deposition was localized at the front of the substrate, showing that the precursor was quickly depleted during deposition. Scanning electron microscopy (SEM) of the gold films deposited at all three temperatures showed that the films were particulate rather than continuous. Within the first 2 mm of each film, island growth morphology was evident (Figure 1). Islands of over 1 μm in size can be seen. Moving along each substrate, the morphology changed; spherical and rodlike particles with a very wide size and shape distribution were observed. UV−vis spectroscopy revealed surface plasmon resonance (SPR) peaks in films deposited at all three temperatures, shown in Figure 2. The SPR peak maximum increased in wavelength, and the peak became broader with increasing deposition temperature. These changes suggest an increase in size or a decrease in particle separation, or both, with higher temperature. XRD confirmed the presence of crystalline cubic gold at all deposition temperatures. Figure 3 shows a typical XRD pattern obtained from a gold film. Within the range measured, two fcc gold peaks are observed: peaks at 2θ values of 38.4° and 44.2° were indexed to the (111) and (200) planes ($a = 4.07$ Å).[26] These are the only peaks expected for cubic gold in the range shown. The broad amorphous background peak centered around 25° is due to the underlying glass substrate. Scherrer analysis of these XRD peaks gave gold crystallite sizes in the range 14−17 nm, although the gold particles present in the sample may be polycrystalline, and therefore of larger size. XRD peak positions and FWHM were invariant along the length of the substrate in each film, although there was a slight reduction in the FWHM at higher deposition temperatures, indicating larger crystallite sizes. X-ray photoelectron spectroscopy (XPS) was carried out on the gold film deposited at 500 °C, and indicated a single gold environment with Au $4f_{5/2}$ and $4f_{7/2}$ binding energies of 87.7 and 84.0 eV, respectively. This environment corresponds to metallic gold. XPS also detected the presence of tin and oxygen from the underlying substrate, and carbon. No other elements were detected; the absence of chlorine and the single gold environment indicate that no unreacted precursor or reaction byproducts remained on the substrate.

The precursor concentration was varied by changing the volume of solvent used, with the total amount of [$HAuCl_4$] being kept constant at 0.080 g, 0.2 mmol. Depositions were carried out with 12.5, 25, 50, 100, and 200 mL of methanol (gold concentrations of 16.3, 8.1, 4.1, 2.0, and 1.0 mM, respectively). Films deposited at all concentrations appeared very similar to the eye: continuous, smooth, nonpowdery, and nonhazy. In each case, the first 70−80 mm of the substrate was coated. The color of the films appeared to change when viewed in transmitted light (lit from the rear) or reflected light (lit from the front). Films were deep blue in transmission with a gold metallic luster when viewed in reflected light. In the first 10−15 mm, the coating appeared yellow-gold in color, similar to bulk gold. SEM of gold films deposited at high concentration showed a profusion of spherical and rodlike particles throughout the length of the film. In contrast, the film deposited at the lowest concentration showed predominantly island growth morphology (Figure 1). Side-on SEM showed that the maximum film thickness in each case was in the range 700−800 nm and was located at the front edge of the substrate, closest to the

(26) Yang, Y.; Shi, J.; Huang, W.; Dai, S.; Wang, L. *J. Mater. Sci.* **2003**, *38*, 1243.

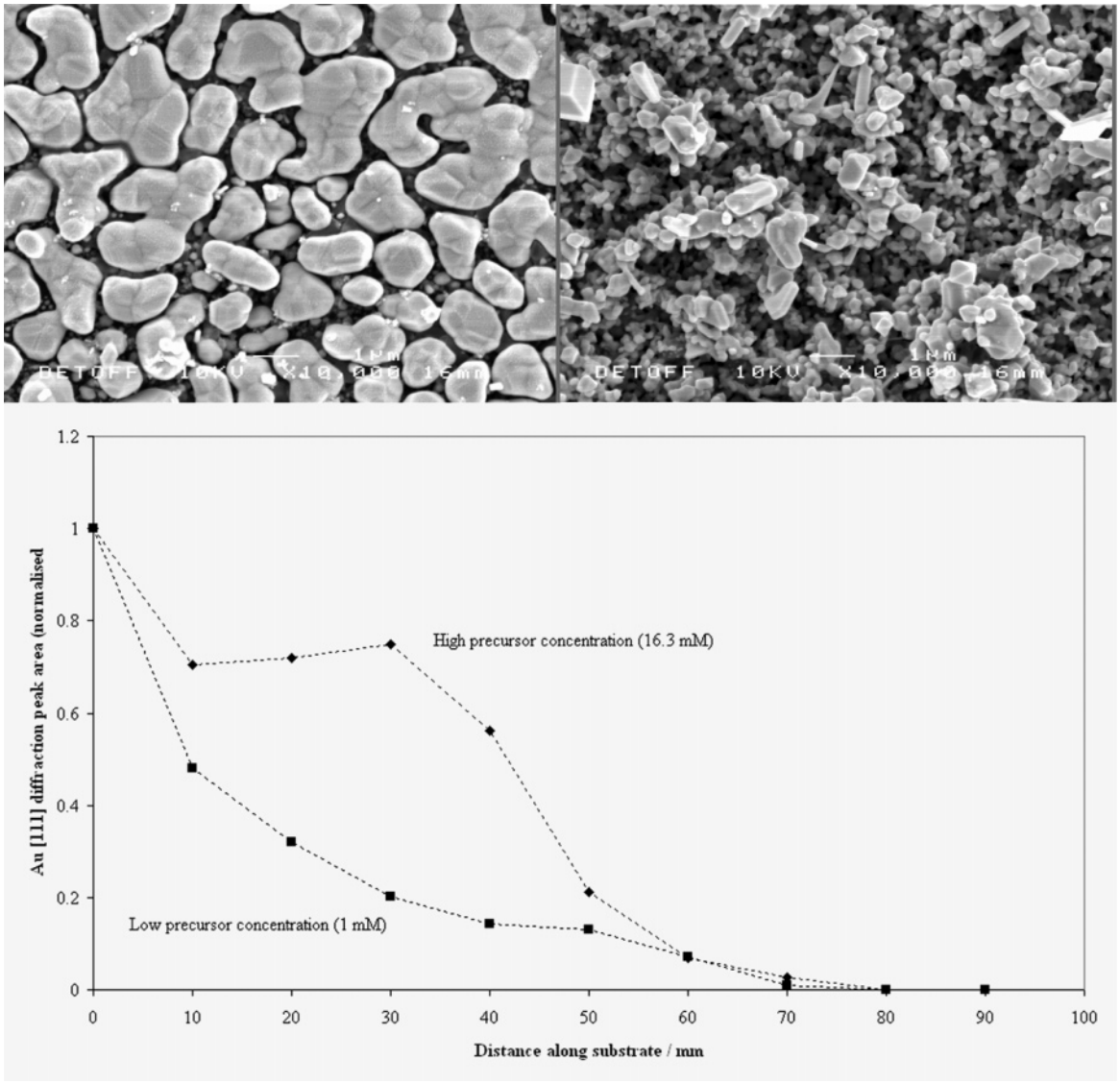

Figure 1. SEM images of a film deposited from [$HAuCl_4$] showing distinctly different morphologies (top). Island growth morphology, favored by low precursor concentration and low deposition temperature (left). Particulate morphology favored by high precursor concentration and high deposition temperature (right). Deposition profile of gold films deposited from $HAuCl_4$ solutions of different concentrations (bottom). At low concentration, the film thickness decreases exponentially along the length of the film. At high concentration, a more complex deposition profile is observed.

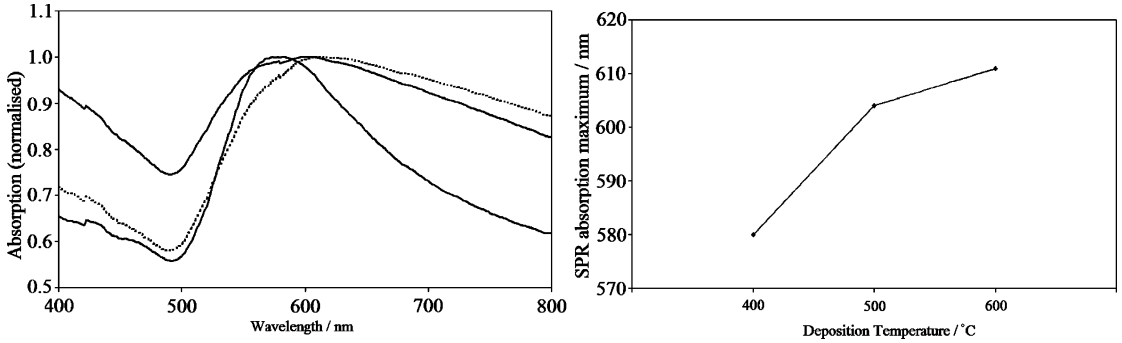

Figure 2. Normalized visible absorption spectra of gold films deposited at different temperatures (left). The surface plasmon resonance (SPR) absorption is evident in each film, and the SPR maxima increase in wavelength with increasing deposition temperature, indicating larger particles (right).

aerosol inlet. Powder XRD conducted at a glancing angle confirmed the presence of crystalline gold in films produced from all concentrations of precursor. The area of the Au-(111) peak was measured at regular intervals along the substrate, starting from the end closest to the aerosol inlet; in this way, the deposition profile was approximated (see Experimental Section for full details). Figure 3 shows a sample XRD pattern taken from a gold film. The peak areas were normalized to the maximum value for each sample, to facilitate comparison between films. This method of profiling assumes that the crystal texture is constant throughout the film. The ratio of the integrated areas of the (111) to (200) peaks was roughly constant throughout each film, suggesting that this is a reasonable approximation to make. The actual

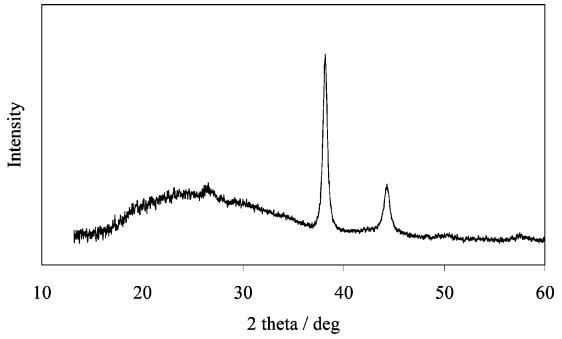

Figure 3. Grazing incidence XRD pattern taken from a gold film deposited from $HAuCl_4$. The broad amorphous background is due to the underlying glass substrate.

film thickness will be affected by the porosity of the film, which is not taken into account by the XRD profiling method. In all cases, the deposition was greatest at the front of the substrate, and reached zero 80−90 mm from the aerosol inlet, indicating depletion of the precursor. There was a marked difference in deposition profile between these two points. At low precursor concentration, the deposition profile along the substrate resembles an exponential decrease (Figure 2). At the highest precursor concentration, the deposition profile shows a distinct local maximum, suggesting a separate deposition process. This may be related to the profusion of spherical and rodlike particles observed by SEM in films deposited from high concentration precursors.

Nanocomposite Films. Nanocomposite films were deposited according to the conditions shown in Table 1. Three series of films were studied. Each series comprised several films with the same metal oxide matrix but with different concentrations of gold. Films are labeled MX, where M denotes the transition metal oxide matrix (M = Ti, Mo, W) and X is an ordinal number indicating the position of the film within the series, with higher numbers indicating greater precursor concentrations of gold. Note that X does not quantitatively describe the precursor gold concentration (see Table 1).

First, some general comments on the appearance of the films. All films appeared smooth and continuous, without visible pin holes or other defects. All films were transparent, with no discernible haze or light scattering. Transmitted and reflected colors, observed visually by front- or back-lighting of the films, were often very different. Each film showed, to some extent, goldlike reflectivity, which increased in prominence within each series at higher gold concentrations. Films were generally mechanically robust as is typical of CVD films. However, at high gold concentrations some films could be damaged by wiping with a tissue or scratching with a scalpel.

Second, by way of comparison between the deposition of gold-only films and gold composite films, it is interesting to note that the presence of a second precursor significantly reduced the temperature required for deposition of gold. For example, no gold film was produced when aerosol assisted CVD was attempted at 200 °C using $[HAuCl_4]$ alone dissolved in methanol. However, in the presence of $[Mo(CO)_6]$, and otherwise under the same conditions, a composite film is formed with strong SPR optical properties, indicating the presence of a substantial metallic gold phase. This indicates that some interaction between the precursors occurs, possibly in the form of increased gas-phase reaction of $[HAuCl_4]$.

Titanium Dioxide/Gold Films. The titanium dioxide/gold composites (films Ti1, Ti2, Ti3) appeared blue in transmitted light and red with a metallic luster in reflected light. The intensity of both the transmitted and reflected color increased from Ti1 to Ti3. Figure 4 shows UV−vis absorption spectra and visible−near-IR reflectance spectra for films Ti1, Ti2, and Ti3. The SPR absorption can be seen centered around 610 nm in all three films. There is little change in the position of the SPR peak with increasing gold precursor concentration, although there is a marked increase in intensity of the absorption. The reflection profile changes significantly with increasing gold concentration. Ti1 shows a narrow reflectance peak centered on 610 nm. Ti2 and Ti3, with higher gold concentrations, show broader, more intense reflectance peaks, with tails extending into the near-IR region. For comparison, the bare silica glass substrate shows a reflectance of around 8% throughout the visible and near-IR region (400−2500 nm).

XPS indicated the presence of Au, Ti, and O in Ti1, Ti2, and Ti3. Carbon contamination was observed on the surface of each film, although this was significantly reduced by argon ion etching. After 30 s of etching, the carbon level fell below 5 atom % for each film, showing that the decomposition of the precursors is relatively clean. Gold was observed in a single environment with $4f_{5/2}$ and $4f_{7/2}$ binding energies of 87.6 and 84.0 eV, corresponding to metallic gold. Ti was also observed in a single environment, with Ti $2p_{1/2}$ and $2p_{3/2}$ binding energies of 464.8 and 459.0 eV. These corresponded well to literature values for the Ti^{4+} ion in TiO_2. Figure 5 shows XPS spectra for Ti3. The absence of a Ti^{3+} environment indicates that the blue color of the films is not caused by a partially reduced titanium oxide phase, suggesting that the color is caused by nanoscale gold particles. The relative amounts of gold and titanium were quantified by integrating the XPS peaks using the Shirley method. The gold composition within the film rose with increasing gold precursor concentration. Au:Ti ratios of 0.10, 0.13, and 0.54 were determined for films Ti1, Ti2, and Ti3, respectively. For films Ti1 and Ti2, the precursor Au:Ti ratio is very similar to the deposited Au:Ti ratio (Table 1).

XRD confirmed the presence of cubic metallic gold in all TiO_2/Au films. Diffraction peaks at 2θ values of 38.3° and 44.5° were observed which arise from the (111) and (200) planes of the Au cubic lattice ($a = 4.07$ Å).[26] No crystalline TiO_2 peaks were observed in the films as deposited, indicating that the crystallinity of the matrix is low. The FWHMs of the Au peaks were almost constant (within 0.5°) along the length of the substrate, indicating roughly constant crystallite size. The ratio of the integrated areas of the (111) to (200) peaks is invariant, within error, showing no change in preferred orientation of the crystalline gold phase. SEM revealed roughly spherical features on the surface of the Au:TiO_2 films. Figure 6, panel A, shows an SEM image of film Ti3. Spherical and near spherical particles of 50−100 nm in diameter can be distinguished on the surface of the film,

Table 1. Deposition Conditions and Optical Properties of Several Series of Gold/Semiconductor Composite Thin Films[a]

sample name	metal oxide precursor, amount/mmol	$HAuCl_4$ amount/mmol	Au:M precursor ratio	solvent	deposition temperature/°C	SPR absorption, λ_{max}/nm	reflectance maximum, λ_{max}/nm
Ti1	$Ti(O^iPr)_4$, 2	0.2	0.10	toluene	400	611	610
Ti2	$Ti(O^iPr)_4$, 2	0.3	0.15	toluene	400	605	720
Ti3	$Ti(O^iPr)_4$, 2	0.6	0.30	toluene	400	612	776
W1	$W(CO)_6$, 1.5	0.05	0.03	methanol	200	547	584
W2	$W(CO)_6$, 1.5	0.1	0.06	methanol	200	557	562
W3	$W(CO)_6$, 1.5	0.2	0.13	methanol	200	579	642
W4	$W(CO)_6$, 1.5	0.4	0.26	methanol	200	584	748
Mo1	$W(CO)_6$, 1.1	0.025	0.02	acetone	200	631	710
Mo2	$Mo(CO)_6$, 1.1	0.05	0.05	acetone	200	631	660
Mo3	$Mo(CO)_6$, 1.1	0.1	0.09	acetone	200	635	676
Mo4	$Mo(CO)_6$, 1.1	0.2	0.18	acetone	200	658	718

[a] Chemical vapor deposition conditions used to deposit nanocomposite thin films of various compositions. Sample names beginning Ti, W, and Mo refer to Au:TiO_2, Au:WO_3, and Au:MoO_3 films, respectively. The surface plasmon resonance absorption maximum and reflectance maximum are also tabulated for each film.

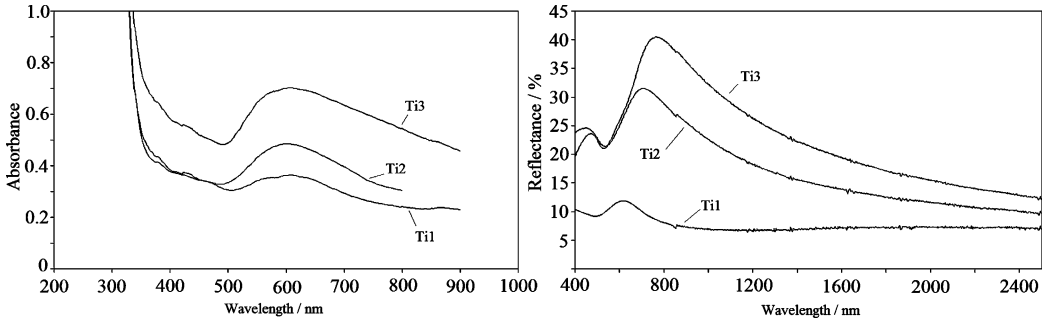

Figure 4. Visible absorption spectra (left) and reflectance spectra (right) of Au:TiO_2 composite films (Ti1, Ti2, Ti3) with an increasing concentration of gold (from bottom to top). The position of the SPR maximum is relatively invariant with increasing concentration, although the reflectivity increases significantly in the red and near-IR regions.

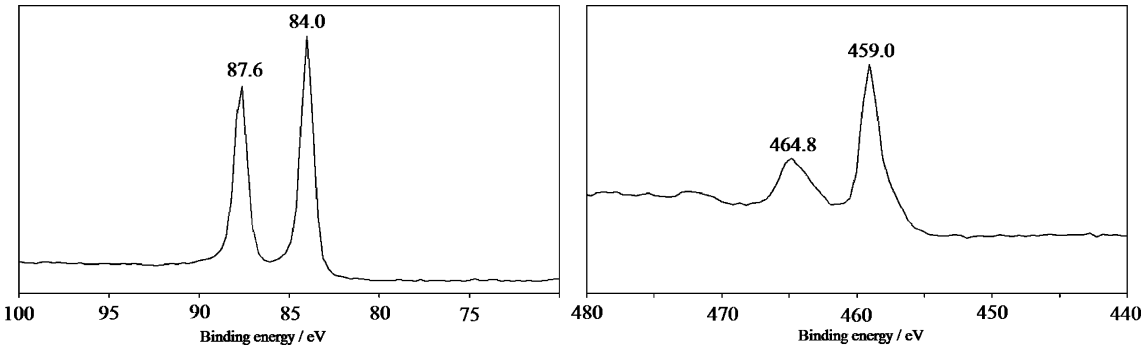

Figure 5. X-ray photoelectron spectra of an Au:TiO_2 composite film. The Au 4f region, showing a single gold environment corresponding to metallic gold (left). The Ti 2p region showing Ti peaks corresponding to TiO_2 (right).

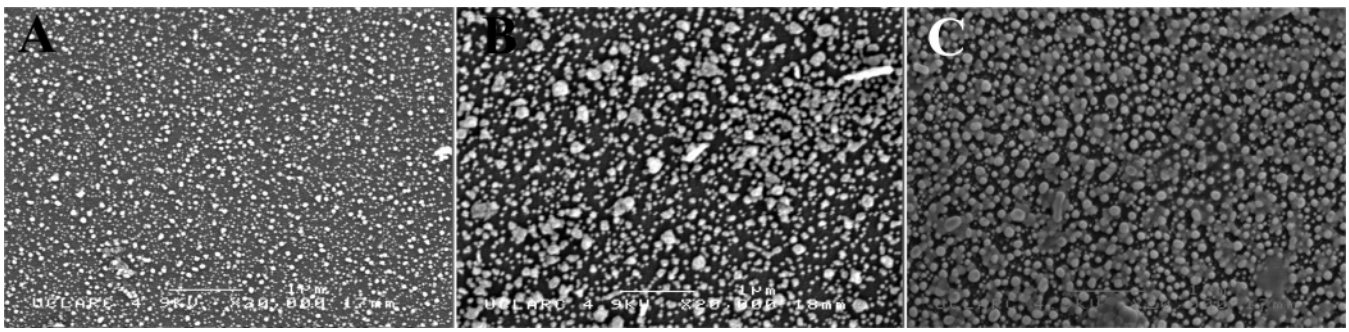

Figure 6. SEM images of metal oxide/gold composite films: Au:TiO_2 (A); Au:WO_3 (B); Au:MoO_3 (C). Scale bars measure 1 μm.

which are interpreted as gold particles embedded in a TiO_2 film. Notably, the gold island growth morphology which was observed in the gold-only films is entirely absent in the composite films. If, as hypothesised earlier, this morphology was formed by surface reaction of [$HAuCl_4$] via conventional CVD growth mechanisms, its absence suggests suppression of these mechanisms, either through lower surface mobility or greater gas-phase reaction of the gold precursor. The increased gas-phase reaction of $HAuCl_4$ in the presence of [$Ti(O^iPr)_4$] or its decomposition products may explain the

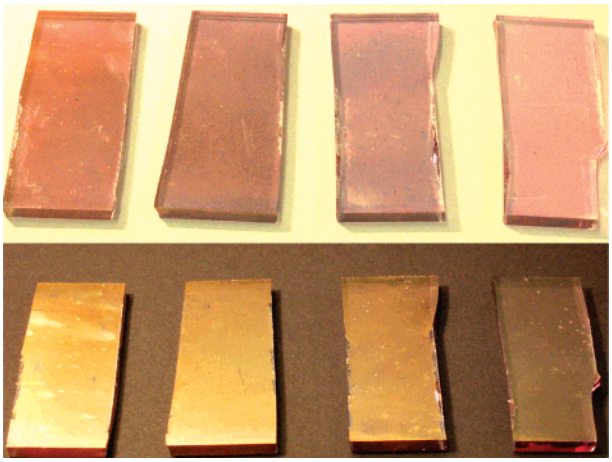

Figure 7. Photographs of tungsten oxide/gold composite films taken lit from the back (top) and from the top (bottom). Films increase in gold concentration from right to left.

lower temperatures necessary to deposit gold when mixed with a second precursor.

Tungsten Oxide and Molybdenum Oxide/Gold Films. The transmitted color of tungsten oxide/gold composites (films W1, W2, W3, W4) varied according to gold concentration. Figure 7 shows photographs of tungsten oxide/gold composite films with different concentrations of gold; lower concentration films appeared red, and higher concentration films appeared blue-purple. In reflection, all films appeared red with a metallic luster. Figure 8 shows the normalized UV−vis absorption spectra and visible−near-IR reflectance spectra for films W1, W2, W3, and W4. All films show an SPR peak, which varies significantly with gold concentration from 546 nm in film W1 to 584 nm in film W4. The reflectance spectra show a similar trend to that observed in the TiO_2/Au series. At low gold concentrations (W1, W2), a discreet reflection peak at around 570 nm was observed. At higher gold concentrations, the peak becomes broader and more intense, and it shifts to longer wavelengths with a tail extending into the near-IR region. In the case of W4, a high reflectance (>20%) persists up to 2500 nm; this reflectance spectrum is distinctly metal-like.[5] XPS indicated the presence of Au, W, and O in all Au:WO_3 films. Gold was observed in a single environment with $4f_{5/2}$ and $4f_{7/2}$ binding energies of 83.9 and 87.6 eV, corresponding to metallic gold. W was observed in a multiple environments, indicating a substoichiometric WO_{3-x} structure. This has been previously observed in tungsten oxide films deposited by CVD through a wide range of conditions.[27−29] SEM indicated a particulate structure (Figure 6, panel B) similar to that observed in the Au:TiO_2 films. Gold particles sizes were difficult to ascertain due to incorporation within the semiconductor film, but they appeared to be in the region of 50−150 nm in diameter.

Molybdenum oxide/gold composites typically displayed regions of different color in the same film. Regions appearing red, blue, and brown to transmitted light were present in all films. These red and blue regions appeared red with a metallic luster in reflected light. XPS indicated the presence of Au and Mo both in single environments, corresponding to metallic gold and MoO_3, respectively. Gold was present throughout the film, in the red, blue, and brown regions, although the concentration varied widely within a single film. In the film Mo2, the Au:Mo atomic ratio at the surface (determined by XPS) varied from 0.52 in the blue region, to 0.20 in the red region, to 0.07 in the brown region, indicating that the different transmitted colors are due to different gold concentrations. SPR absorption peaks were present in all films in the blue and red regions. The brown regions showed no plasmon peak. In the red region, the SPR peak was observed around 560 nm in all four films. Figure 9 shows the reflectance and absorption spectra for the blue regions of Mo1 to Mo4. In the blue region, SPR varied in wavelength with increasing gold concentration from 631 nm (Mo1) to 658 nm (Mo4). SEM (Figure 6, panel C) of film Mo4 shows spherical particles, with some elongated rods, partially surrounded by a matrix.

Discussion

To the very best of our knowledge, this report is the first example of CVD carried out using [$HAuCl_4$] as a precursor. As has been previously noted, [$HAuCl_4$] is not easily vaporized due to its low decomposition temperature, and so is unsuitable for variants of CVD in which the precursor is transported in the vapor phase. However, apart from its low volatility, [$HAuCl_4$] has the characteristics of an excellent CVD precursor. The thermal decomposition reaction (shown in the introduction) leads to the desired solid phase with only gaseous byproducts (HCl and Cl_2). XPS showed no chlorine contamination in any film, and only metallic gold was observed, showing that the decomposition of the precursor was complete. The absence of Cl at any detectable level in films produced from [$HAuCl_4$] shows that the decomposition is clean, and the byproducts are effectively removed from the substrate.

When deposited alone, [$HAuCl_4$] formed films showing separate regions of island growth morphology and highly particulate morphology. Films consisting entirely of island growth morphology could be produced by using a low precursor concentration, while highly particulate films resulted from the use of high precursor concentration. Deposition profiles were determined by XRD, as described above. In the case of low precursor concentration, this analysis showed an exponential-like decay of the film thickness with distance along the substrate. This corresponds to an exponential decrease in the reaction rate with residence time in the reactor. In the case of high precursor concentrations, a distinctly different deposition profile is observed, with a local deposition maximum around halfway along the film's length (Figure 1). This more complex profile suggests a more complex mechanism; SEM imaging points to the increased formation of spherical and rodlike particles at higher precursor concentrations, which either cover or replace the island growth morphology observed with low precursor concentration. These particles are likely to be a result of gas-phase reaction, which would be favored by high precursor concentrations. The SEM and XRD evidence therefore

(27) Ashraf, S.; Blackman, C. S.; Palgrave, R. G.; Parkin, I. P. *J. Mater. Chem.* **2007**.
(28) Blackman, C. S.; Parkin, I. P. *Chem. Mater.* **2005**, *17*, 1583.
(29) Hussain, Z. *J. Mater. Res.* **2001**, *16*, 2695.

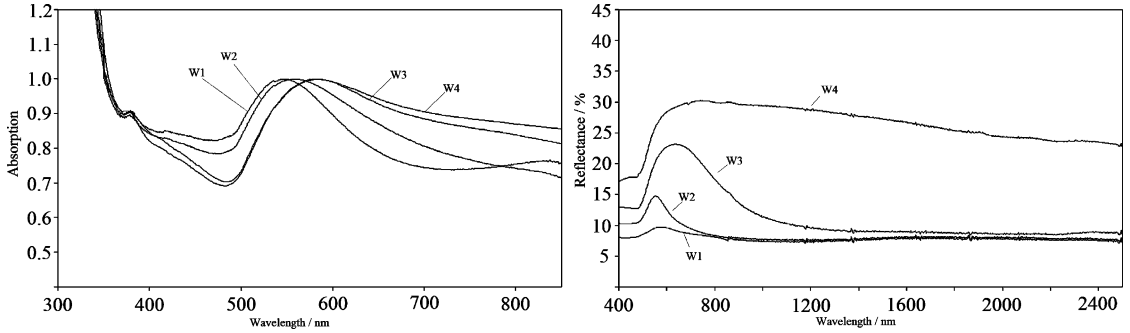

Figure 8. Normalized visible absorption spectra (left) and reflectance spectra (right) of Au:WO_3 composite films (W1, W2, W3, W4). The wavelength of the SPR maximum increases with increasing concentration, and the reflectivity increases significantly in the red and near-IR regions. The highest concentration film (W4) shows a high reflectivity throughout the red and near-IR region that is distinctly metal-like.

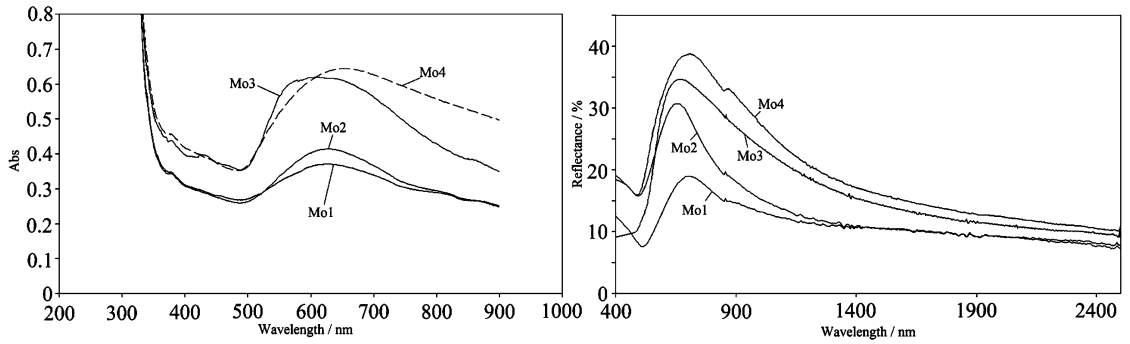

Figure 9. Normalized visible absorption spectra (left) and reflectance spectra (right) of Au:MoO_3 composite films (Mo1, Mo2, Mo3, Mo4). The absorption spectrum for Mo4 is dashed for clarity.

suggests a mechanism whereby, at high precursor concentration, gas-phase nucleation is favored, and the film morphology is highly particulate. At low precursor concentration, gas-phase reaction is minimal, surface reaction is favored, and island growth morphology results.

In composite films, the island growth morphology was not observed, indicating the suppression of the surface reaction mechanism. This could be due to a lower surface mobility of the gold precursor, due to alterations in the surface chemistry and morphology caused by the growing semiconductor film. Alternatively, the gas-phase reaction of [$HAuCl_4$] could be enhanced by the presence of a second precursor, leading to extensive gas-phase nucleation. In the nanocomposite films, the gold particles have a wide size distribution, and the films are nonuniform on the micron scale making precise optical tailoring difficult. Mulvaney et al. studied films of Au@SiO_2 core−shell particles, the gold cores of which showed dipole interaction.[8,9] In their work, the Maxwell−Garnett (MG) model was used to successfully predict the optical properties of dense arrays of gold particles which were kept physically separate by their surrounding layers of silica. This structure bears a resemblance to the nanocomposite materials produced in this work, where gold particles are also separated by a dielectric material. The materials produced in this work show greater particle polydispersity. This can be explained by the nature of their formation in a CVD environment, rather than a more controlled solution-phase synthesis. Despite this, qualitative trends can be identified in the plasmon properties of the films reported here. The SPR characteristics of the nanocomposite films can be adjusted rationally by changing the gold:metal oxide precursor ratio. At higher concentrations of gold, the SPR absorption peak is red-shifted and broadened. Correspondingly, the reflectance peak, which begins as a small localized peak at low concentrations, is red-shifted and increased in intensity. In films with a higher concentration of gold, the near infrared reflectance reaches relatively high values (around 30%), and metal-like reflectivity is observed. It has therefore been shown that the absorption and reflectance properties of the composite materials can be influenced through the simple adjustment of the precursor ratios. The refractive index of the matrix is also shown to influence the SPR. Mie theory and MG theory both predict a red-shifting of the SPR peak with increasing refractive index of the surrounding medium. The refractive index of the matrix materials taken from literature measurements on bulk anatase-TiO_2, MoO_3, and WO_3 are 2.4, 2.2, and 1.8, respectively.[29,30] The ranges of SPR absorption peaks observed for gold particles within TiO_2, MoO_3, and WO_3 matrices were 605−612, 631−658, and 547−584 nm, respectively. The MoO_3 composites show SPR peaks significantly red-shifted compared to those observed in the WO_3 composites. This is in accord with the significantly higher refractive index of MoO_3. However, on the basis of refractive index, TiO_2 composite films would be expected to show an SPR peak red-shifted still further. In fact, the peaks are observed to be blue-shifted compared to those of the MoO_3 composites. This could be due to the low crystallinity of the TiO_2 matrix, as observed by XRD, which would significantly alter the refractive index of the material.

While the composites produced in this work do not show the uniformity of those produced by layer-by-layer deposition

(30) Hussain, Z. *Appl. Opt.* **2002**, *41*, 6708.

technique, they do have the advantage of a simple, single step deposition, using a technique that may be adaptable to large scale industrial production, while still retaining a good degree of control over optical properties.

Conclusions

In conclusion, hydrogen tetrachloroaurate [$HAuCl_4$] proved to be an excellent precursor to metallic gold, avoiding many of the difficulties encountered with previous gold CVD precursors, such as air-sensitivity and high cost. A wide range of conditions can be used to deposit gold films. High substrate temperature and precursor concentration favored a particulate morphology, while the opposites favored island growth morphology. Nanocomposite films can also be deposited by combining [$HAuCl_4$] with conventional precursors. The optical properties of these films can be rationally tuned by changing the ratio of the precursors. The AACVD method has therefore proved to be a versatile route to produce a variety of nanostructured thin films with easily tunable optical properties.

Acknowledgment. The authors thank S. Ashraf, P. Kerr, Dr. R. Binions, and Dr. C. Blackman for helpful discussions. This research was partially supported by a studentship awarded to R.G.P. from the Department of Chemistry, University College London. I.P.P. is a Wolfson-Royal Society Merit Award holder.

CM0629006